

Electrostatic patch effects in Casimir-force experiments performed in the sphere-plane geometryR. O. Behunin,^{1,2} Y. Zeng,² D. A. R. Dalvit,² and S. Reynaud³¹*Center for Nonlinear Studies, Los Alamos National Laboratory, Los Alamos, New Mexico 87545, USA*²*Theoretical Division, MS B213, Los Alamos National Laboratory, Los Alamos, New Mexico 87545, USA*³*Laboratoire Kastler Brossel, CNRS, ENS, UPMC, Campus Jussieu, F-75252 Paris, France*

(Received 10 July 2012; published 16 November 2012)

Patch potentials arising from the polycrystalline structure of material samples may contribute significantly to measured signals in Casimir force experiments. Most of these experiments are performed in the sphere-plane geometry; yet, up to now all analysis of patch effects has been taken into account using the proximity force approximation which, in essence, treats the sphere as a plane. In this paper we present the exact solution for the electrostatic patch interaction energy in the sphere-plane geometry and derive exact analytical formulas for the electrostatic patch force and minimizing potential. We perform numerical simulations to analyze the distance dependence of the minimizing potential as a function of patch size, and we quantify the sphere-plane patch force for a particular patch layout. Once the patch potentials on both surfaces are measured by dedicated experiments our formulas can be used to exactly quantify the sphere-plane patch force in the particular experimental situation.

DOI: [10.1103/PhysRevA.86.052509](https://doi.org/10.1103/PhysRevA.86.052509)

PACS number(s): 31.30.jh, 12.20.-m, 42.50.Ct, 78.20.Ci

I. INTRODUCTION

In distinction to what one is taught in introductory physics courses, the surfaces of real metals are not equipotentials but are rather described by a locally varying surface voltage, known simply as patch potentials. Patch potentials exist for several reasons. One is that the work function of a crystalline structure depends upon which crystallographic plane an electron is extracted from [1,2]. Real metal surfaces are typically composed of a network of crystallites with random crystallographic orientations, thereby giving rise to a nonuniform potential over the metal's surface. In addition, surface contamination by adsorbates is well-known experimentally [3–6] and theoretically [7] to lead to changes in the work function. Even for monocrystalline surfaces a spatially varying potential has been observed [8]. Patch potentials have important implications in various experimental disciplines, including gravitational measurements on elementary charged particles [9], tests of the general theory of relativity [10–13], ion trapping [14–16], and the physics of Rydberg atoms [8,17]. In this paper we focus on the effects that electrostatic patches can have on measurements of the Casimir force [18–23].

Most Casimir force measurements to date have been performed in the sphere-plane geometry in order to skirt alignment difficulties. The electrostatic interaction is used to calibrate the system and to determine the absolute separation between the sphere and the plane. In the idealized case of equipotential surfaces, i.e., no patches on the surfaces, the exact analytical expression for the sphere-plane electrostatic force (the Coulomb force) is well known [24], valid for arbitrary values of the ratio D/R , where D is the sphere-plane separation and R is the radius of the sphere. In typical experiments $D/R \ll 1$, and the exact expression reduces to its proximity force approximation (PFA). This approximation replaces the sphere by infinitesimal planar surface elements and computes the electrostatic force by adding plane-plane contributions, as if they were independent. For nonequipotential surfaces PFA has also been used to compute the electrostatic patch force between the sphere and the plane [18,19,22,23]. A further assumption in the computation of

patch effects has been the ergodic hypothesis, which assumes that the actual realization of patches on both surfaces can be well represented by statistical properties of their sizes, shapes, and voltages. Since the sphere has a compact cross section the sphere-plane interaction can be characterized by an effective area of interaction, and the ergodic hypothesis is expected to be satisfied when there are many patches within the interaction area, thereby providing a fair representation of the patches' statistical properties.

The main goal of this paper is to derive the exact analytical expression for the sphere-plane electrostatic patch force which to the best of our knowledge has not yet been reported in the literature. Previous theoretical [19,21,22] and experimental [25,26] works have used PFA to address the implications of patch potentials on the electrostatic calibration process for Casimir force measurements. In this paper we also address the same issue using our exact expression for the sphere-plane electrostatic patch force.

Measurements of the Casimir force between vacuum-separated bodies rely on an electrostatic calibration which is performed by sweeping through various values of an externally applied potential between the bodies. This procedure generates a parabolic force curve as a function of applied voltage, the minimum of which identifies the minimizing potential. In the absence of patches, the minimizing potential is independent of D , and an external voltage equal to the minimizing potential allows for the nullification of all electrostatic forces. However, when patches are present this is no longer the case. As we show below using our exact expression for the sphere-plane patch force, the presence of patches on the samples implies that there is no external voltage that can nullify the electrostatic interaction—at most the force can be minimized by applying a voltage equal to the minimizing potential. Also, the existence of patches implies that this minimizing potential is, in general, a function of sphere-plane distance D . However, we show that when many patches are contained within the effective area of interaction the spatial variation of the minimizing potential is suppressed. In this regime the minimizing potential may appear, in experiment, to be distance independent. Even in this situation the residual electrostatic force is nonzero.

With a detailed knowledge of the patch potentials on the sphere and plane surfaces, to be provided by dedicated ongoing and future measurements, the results contained here can be used to exactly quantify the contribution of electrostatic patches to measured signals in Casimir force experiments.

II. EXACT SPHERE-PLANE PATCH FORCE

We seek the solution to the boundary value problem for the electrostatic potential $V(\mathbf{x})$ in the space between the sphere and the plane. The potential satisfies the Laplace equation

$$\nabla^2 V(\mathbf{x}) = 0, \quad (1)$$

subject to the following boundary conditions:

$$V(\mathbf{x})|_{\mathbf{x} \in \mathbf{P}} = V_p(\mathbf{x}), \quad V(\mathbf{x})|_{\mathbf{x} \in \mathbf{S}} = V_s(\mathbf{x}). \quad (2)$$

Here $V_p(\mathbf{x})$ and $V_s(\mathbf{x})$ are the potentials on the plane and the sphere, respectively, and \mathbf{P} and \mathbf{S} denote the set of points belonging to the plane and the sphere, respectively. Once we have the solution for the potential we can calculate the electric field, $\mathbf{E} = -\nabla V$, and thus the electrostatic energy in the sphere-plane configuration

$$E_{\text{sp}} = \frac{\varepsilon_o}{2} \int_{\mathcal{V}} d^3 \mathbf{x} (\nabla V)^2, \quad (3)$$

where \mathcal{V} denotes the volume between the sphere and the plane, and ε_o is the permittivity of vacuum. Finally, the electrostatic sphere-plane force is obtained by taking the gradient of the energy, $\mathbf{F}_{\text{sp}} = +\nabla E_{\text{sp}}$.

In the following subsections we outline the techniques used to arrive at the exact solution for the potential given general electrostatic patchy boundary conditions, the resulting interaction energy and force, and finally the minimizing potential. To this end we make use of bispherical coordinates [27]. The key advantages of the bispherical coordinate system for this problem are that the Laplacian separates and the two surfaces on which we define our boundary conditions are described by constant coordinate surfaces.

A. Electrostatic patch energy—Bispherical coordinates

Bispherical coordinates (η, ξ, ϕ) can be used to label each point in \mathbb{R}^3 . The correspondence with Cartesian coordinates is given by the following relations:

$$\begin{aligned} x &= \frac{a \sin \xi \cos \phi}{\cosh \eta - \cos \xi}; & y &= \frac{a \sin \xi \sin \phi}{\cosh \eta - \cos \xi}; \\ z &= \frac{a \sinh \eta}{\cosh \eta - \cos \xi}. \end{aligned} \quad (4)$$

See Figure 1 for a visual representation. For the sphere-plane geometry the adoption of bispherical coordinates leads to a significant simplification of the expression of the energy through the use of Gauss' divergence theorem in curvilinear coordinates:

$$\begin{aligned} E_{\text{sp}} &= \frac{\varepsilon_o}{2} \int_{\mathbf{P}} d\mathbf{a} \cdot \mathbf{E}(\eta = 0, \xi, \phi) V_p(\xi, \phi) \\ &\quad - \frac{\varepsilon_o}{2} \int_{\mathbf{S}} d\mathbf{a} \cdot \mathbf{E}(\eta = \Lambda, \xi, \phi) V_s(\xi, \phi), \end{aligned} \quad (5)$$

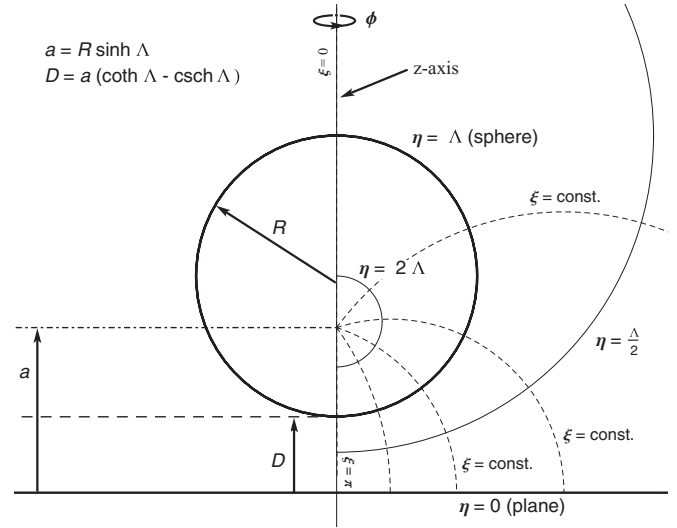


FIG. 1. Slice of the bispherical coordinate system along the z axis. The solid lines are η -constant surfaces, and the dashed lines represent ξ -constant surfaces. To span \mathbb{R}^3 the coordinate system pictured above is rotated about the z axis; the η -constant ($\eta \neq 0$) surfaces will sweep out spheres and the ξ -constant surfaces will sweep out “apples” for $0 < \xi < \pi/2$ and “lemons” for $\pi/2 < \xi < \pi$. The cross section of the $\eta = \Lambda$ surface corresponds to the sphere, and $\eta = 0$ is the plane. The relations between the geometrical parameters D and R and the bispherical parameters a and Λ are indicated in the figure.

where E_η is the η component of the electric field and $d\mathbf{a} = \sqrt{\Sigma(\eta)} d\xi d\phi \hat{\eta}$ is the oriented measure for the integration over an η -constant surface. The factor $\sqrt{\Sigma(\eta)} = (a^2 \sin \xi) / (\cosh \eta - \cos \xi)^2$ is the square root of the determinant of the metric induced on an η -constant surface. In these coordinates it is useful to relate Λ (the η coordinate for the sphere) and a (the location of the foci of the bispherical coordinate system) to the radius of the sphere R and the sphere-plane separation D :

$$\begin{aligned} \cosh \Lambda &= 1 + D/R, \\ a &= \sqrt{(D + R)^2 - R^2} = R \sinh \Lambda. \end{aligned} \quad (6)$$

The Laplacian of the potential in these coordinates is

$$\begin{aligned} \nabla^2 V &= \frac{(\cosh \eta - \cos \xi)^3}{a^2 \sin \xi} \left[\frac{\partial}{\partial \eta} \left(g(\eta, \xi) \frac{\partial V}{\partial \eta} \right) \right. \\ &\quad \left. + \frac{\partial}{\partial \xi} \left(g(\eta, \xi) \frac{\partial V}{\partial \xi} \right) + \frac{g(\eta, \xi)}{\sin^2 \xi} \frac{\partial^2 V}{\partial \phi^2} \right], \end{aligned} \quad (7)$$

where $g(\eta, \xi) = \sin \xi / (\cosh \eta - \cos \xi)$. By making the ansatz $V = \sqrt{\cosh \eta - \cos \xi} H(\eta) \Xi(\xi) \Psi(\phi)$ the Laplace equation separates,

$$\begin{aligned} \sin^2 \xi \frac{H''(\eta)}{H(\eta)} + \frac{\Psi''(\phi)}{\Psi(\phi)} - \frac{1}{4} \sin^2 \xi \\ + \sin \xi \cos \xi \frac{\Xi'(\xi)}{\Xi(\xi)} + \sin^2 \xi \frac{\Xi''(\xi)}{\Xi(\xi)} = 0. \end{aligned} \quad (8)$$

To arrive at this equation we have divided through by $\csc^2(\xi)(\cosh \eta - \cos \xi)^{5/2} H(\eta) \Xi(\xi) \Psi(\phi)$. Each of the functions $\Xi(\xi)$, $H(\eta)$, and $\Psi(\phi)$ can be solved for by separation of

variables giving the following general solution:

$$V(\eta, \xi, \phi) = \sqrt{\cosh \eta - \cos \xi} \sum_{l=0}^{\infty} \sum_{k=-l}^l e^{ik\phi} P_l^k(\cos \xi) [A_{lk} e^{\lambda_l \eta} + B_{lk} e^{-\lambda_l \eta}], \quad (9)$$

where $\lambda_l = l + 1/2$, and A_{kl} and B_{kl} are constants to be determined by the boundary conditions on the potential. The function P_l^k is the associated Legendre polynomial [28].

The expansion coefficients are obtained by using the orthonormality properties of the eigenfunctions which serve as the basis for $V(\eta, \xi, \phi)$. By imposing the boundary conditions (2), we find the exact solution for the electrostatic potential with general patchy boundary conditions on the sphere and the plane, namely,

$$V(\eta, \xi, \phi) = \sum_{\ell=0}^{\infty} \sum_{k=-\ell}^{\ell} \frac{\lambda_{\ell}}{2\pi} (-1)^k \int_0^{2\pi} d\phi' \int_0^{\pi} d\xi' \sin \xi' e^{ik(\phi-\phi')} P_{\ell}^k(\cos \xi) P_{\ell}^{-k}(\cos \xi') \\ \times \left[\sqrt{\frac{\cosh \eta - \cos \xi}{\cosh \Lambda - \cos \xi'}} \frac{\sinh \lambda_{\ell} \eta}{\sinh \lambda_{\ell} \Lambda} V_s(\xi', \phi') - \sqrt{\frac{\cosh \eta - \cos \xi}{1 - \cos \xi'}} \frac{\sinh \lambda_{\ell} (\eta - \Lambda)}{\sinh \lambda_{\ell} \Lambda} V_p(\xi', \phi') \right]. \quad (10)$$

Using Eq. (10) the general expression for the electrostatic energy of the sphere-plane system can be written by noting that the η component of the electric field is $E_{\eta} = -a^{-1}(\cosh \eta - \cos \xi)^{\frac{\partial}{\partial \eta}} V(\eta, \xi, \phi)$, where we have used the expression for the gradient in curvilinear coordinates. By combining the result for E_{η} with the expression for the energy (5) we find the general expression for the electrostatic energy:

$$E_{\text{sp}} = \frac{\epsilon_0}{2} R \sinh \Lambda \sum_{\ell=0}^{\infty} \sum_{k=-\ell}^{\ell} \frac{\lambda_{\ell}}{2\pi} (-1)^k \int d\Omega \int d\Omega' e^{ik(\phi-\phi')} P_{\ell}^k(\cos \xi) P_{\ell}^{-k}(\cos \xi') \\ \times \left[\frac{V_s(\Omega) V_s(\Omega')}{\sqrt{\cosh \Lambda - \cos \xi} \sqrt{\cosh \Lambda - \cos \xi'}} \left(\lambda_{\ell} \coth \lambda_{\ell} \Lambda + \frac{\sinh \Lambda}{2(\cosh \Lambda - \cos \xi)} \right) + \frac{V_p(\Omega) V_p(\Omega')}{\sqrt{1 - \cos \xi} \sqrt{1 - \cos \xi'}} \lambda_{\ell} \coth \lambda_{\ell} \Lambda \right. \\ \left. - \frac{V_s(\Omega) V_p(\Omega')}{\sqrt{\cosh \Lambda - \cos \xi} \sqrt{1 - \cos \xi'}} \frac{\lambda_{\ell}}{\sinh \lambda_{\ell} \Lambda} - \frac{V_p(\Omega) V_s(\Omega')}{\sqrt{1 - \cos \xi} \sqrt{\cosh \Lambda - \cos \xi'}} \frac{\lambda_{\ell}}{\sinh \lambda_{\ell} \Lambda} \right]. \quad (11)$$

Here $\int d\Omega$ is the integration over the ‘‘solid angle’’ $\int_0^{\pi} d\xi \int_0^{2\pi} d\phi \sin \xi$, and $V(\Omega) \equiv V(\xi, \phi)$ in bispherical coordinates.

Self-energy terms, both for the sphere and for the plane, are contained within Eq. (11), and their expression in bispherical coordinates can be found by taking the limit of infinite sphere-plane separation $D \rightarrow \infty$. We describe the calculation of these self-energy terms in Appendix A. In order to obtain the sphere-plane electrostatic interaction energy these self-energy terms must be subtracted from the above expression for the energy.

B. Electrostatic patch force

We can find the sphere-plane patch force by taking the derivative of the interaction energy with respect to the separation, $F_{\text{sp}} = (\partial/\partial D) E_{\text{sp}}^{\text{int}}$. The expression for the energy in bispherical coordinates (11) is, however, not very transparent for computing the force. This is due to the fact that in bispherical coordinates the sphere and plane potentials, which prescribe our boundary conditions, are a function of the sphere-plane separation [29]. To circumvent this complication and to connect with the natural basis in which the patch potentials are to be measured, we transform to the natural coordinate system for each body. Therefore, we make the following change of variables (see Appendix A for details of coordinate transformations from bispherical to spherical or

polar coordinates):

$$\int d\Omega V_s(\Omega)(\dots) \rightarrow \int d\Omega_s V_s(\Omega_s) \frac{\sinh^2 \Lambda}{(\cosh \Lambda + \cos \theta)^2}(\dots), \\ \int d\Omega V_p(\Omega)(\dots) \rightarrow \int d\Omega_p V_p(\Omega_p) \frac{4a^2}{(\rho^2 + a^2)^2}(\dots), \quad (12)$$

where $\Omega_s \equiv (\theta, \phi)$ are spherical coordinates on the sphere and $\Omega_p \equiv (\rho, \phi)$ are polar coordinates on the plane. The integration measure $\int d\Omega_s$ is given by $\int_0^{2\pi} d\phi \int_0^{\pi} d\theta \sin \theta$, with θ defined as the polar angle on the sphere, and $\int d\Omega_p = \int_0^{2\pi} d\phi \int_0^{\infty} d\rho \rho$, where ρ is the radius for a polar coordinate system defined on the plane. We can then express the sphere-plane electrostatic interaction energy in terms of the natural basis for the two bodies,

$$E_{\text{sp}} = \sum_{a,b=s,p} \int d\Omega_a \int d\Omega_b V_a(\Omega_a) \mathcal{E}_{a,b}(\Omega_a; \Omega_b; D) V_b(\Omega_b), \quad (13)$$

where all dependence of the energy on the sphere-plane separation is now contained in the kernels $\mathcal{E}_{a,b}(\Omega_a; \Omega_b; D)$. Since the functions $\mathcal{E}_{a,b}(\Omega_a; \Omega_b; D)$ are complicated we place their explicit derivations and expressions in Appendix B. By taking the derivative of the energy equation, Eq. (13), with respect to D , the exact electrostatic patch force between the

sphere and the plane can now be computed as

$$F_{\text{sp}} = \sum_{a,b=s,p} \int d\Omega_a \int d\Omega_b V_a(\Omega_a) \mathcal{F}_{a,b}(\Omega_a; \Omega_b; D) V_b(\Omega_b), \quad (14)$$

where $\mathcal{F}_{a,b}(\Omega_a; \Omega_b; D) = (\partial/\partial D)\mathcal{E}_{a,b}(\Omega_a; \Omega_b; D)$. The force above is general for arbitrary boundary conditions on the sphere and the plane.

It is important to emphasize that in these expressions the origin of the polar coordinate system on the plane is assumed to be right below the sphere, at the point of closest approach between the two bodies. Generally, the measured electrostatic patch potential distribution on the plane will be done with respect to a different coordinate system, say a Cartesian system on the plane. In this case, the appropriate change of coordinate system on the plane must be performed prior to using Eqs. (11) and (14).

In Appendix C we show how to obtain from our exact expressions for the energy equation, Eq. (11), and the force equation, Eq. (14), for patchy boundary conditions the corresponding well-known formulas for the special case of equipotential surfaces.

C. Minimizing potential and residual electrostatic force

As mentioned above, in most Casimir force measurements an external voltage, V_0 , is applied between the two surfaces

to perform the calibration of the system. By sweeping V_0 between positive and negative values, the total interaction force (or its gradient) versus V_0 is measured for fixed sphere-plane separation D , resulting in a force “parabola” vs potential due to the quadratic dependence of F_{sp} on V_0 . These measurements are then repeated for each separation. The minima of each of the parabolas defines the minimizing potential, namely,

$$\left. \frac{\partial F_{\text{sp}}}{\partial V_0} \right|_{V_0=V_{\text{min}}} = 0. \quad (15)$$

An explicit exact expression for the minimizing potential can be found in this way (see also Refs. [19,22] for a similar approach using PFA). To do so we replace in Eq. (14) the patchy potential on the sphere V_s by $V_0 + V_s(\Omega_s)$, i.e., by the addition of the constant applied potential and the nonconstant patchy one. Alternatively, we can do a similar replacement for the patchy potential on the plane and, of course, an identical minimizing potential is obtained. The surface potentials on each of the objects are assumed to fluctuate around the potential given by the average work function of the surface material. For convenience we write the potentials in terms of their average value and a term describing fluctuations around zero. For example, the potential on the sphere becomes $V_s(\Omega_s) = \bar{V}_s + \Delta V_s(\Omega_s)$, where \bar{V}_s denotes the average potential and $\Delta V_s(\Omega_s)$ its fluctuations. By solving Eq. (15) we find

$$\begin{aligned} V_{\text{min}}(D) &= - \frac{\int d\Omega_s \int d\Omega'_s [\bar{V}_s + \Delta V_s(\Omega_s)] \mathcal{F}_{s,s}(\Omega_s; \Omega'_s; D) + \int d\Omega_p \int d\Omega'_p [\bar{V}_p + \Delta V_p(\Omega_p)] \mathcal{F}_{p,s}(\Omega_p; \Omega'_s; D)}{\int d\Omega_s \int d\Omega'_s \mathcal{F}_{s,s}(\Omega_s; \Omega'_s; D)} \\ &= -\bar{V}_s + \bar{V}_p - \underbrace{\frac{\int d\Omega_s \int d\Omega'_s \Delta V_s(\Omega_s) \mathcal{F}_{s,s}(\Omega_s; \Omega'_s; D) + \int d\Omega_p \int d\Omega'_p \Delta V_p(\Omega_p) \mathcal{F}_{p,s}(\Omega_p; \Omega'_s; D)}{\int d\Omega_s \int d\Omega'_s \mathcal{F}_{s,s}(\Omega_s; \Omega'_s; D)}}_{\Delta V_{\text{min}}(D)}. \end{aligned} \quad (16)$$

In the second line above the integrations against the average potentials have been done. This result can be easily understood for the case when there are no patches altogether, $\Delta V_s = \Delta V_p = 0$. In this case the minimizing potential is the applied potential necessary to nullify the force between an equipotential sphere and plane [see Eq. (C9)] and does not depend on D . The integrals against the fluctuating parts of the potential above, $\Delta V_{\text{min}}(D)$, represent a sort of weighted average of the patchy part of the potential and are responsible for all of the spatial dependence of the minimizing potential.

In general, the minimizing potential depends on the sphere-plane separation D through the distance dependency of the kernels $\mathcal{F}_{s,s}$ and $\mathcal{F}_{p,s}$. This is shown explicitly in our numerical examples below, where we also discuss the special conditions under which V_{min} may appear to be distance independent even in the presence of patches. One should also note that, in general, setting the applied potential V_0 equal to the minimizing potential V_{min} does not nullify the electrostatic patch contribution to the total sphere-plane force. This can be seen by evaluating the electrostatic force at $V_0 = V_{\text{min}}$:

$$\begin{aligned} F_{\text{sp}}(V_0 = V_{\text{min}}) &= \sum_{a,b=s,p} \int d\Omega_a \int d\Omega_b V_a(\Omega_a) \mathcal{F}_{a,b}(\Omega_a; \Omega_b; D) V_b(\Omega_b) - V_{\text{min}}^2 \int d\Omega_s \int d\Omega'_s \mathcal{F}_{s,s}(\Omega_s; \Omega'_s; D) \\ &= \sum_{a,b=s,p} \int d\Omega_a \int d\Omega_b \Delta V_a(\Omega_a) \mathcal{F}_{a,b}(\Omega_a; \Omega_b; D) \Delta V_b(\Omega_b) - \Delta V_{\text{min}}^2(D) \int d\Omega_s \int d\Omega'_s \mathcal{F}_{s,s}(\Omega_s; \Omega'_s; D), \end{aligned} \quad (17)$$

which is generally different from zero. The second line shows that the electrostatic calibration completely eliminates the equipotential component of the force, but does not eliminate the fluctuating part. This residual electrostatic force, together with any other voltage-independent interactions (such as the Casimir force), make up the signal in Casimir force measurements.

The expression (17) gives the minimum magnitude that the sphere-plane electrostatic force can take for arbitrary surface potentials ΔV_a . Let us now consider what particular form ΔV_a must take in order to minimize the residual force given by Eq. (17). To do this we will take the variational derivative of $F_{\text{sp}}(V_0 = V_{\text{min}})$ with respect to the surface potentials and set the

result to zero:

$$\begin{aligned}
0 &= \frac{\delta F_{\text{sp}}(V_0 = V_{\text{min}})}{\delta \Delta V_a(\Omega_a)} = 2 \sum_{b=s,p} \int d\Omega_b \mathcal{F}_{a,b}(\Omega_a; \Omega_b; D) \Delta V_b(\Omega_b) - 2 \Delta V_{\text{min}}(D) \int d\Omega_s \int d\Omega'_s \mathcal{F}_{s,s}(\Omega_s; \Omega'_s; D) \frac{\delta \Delta V_{\text{min}}(D)}{\delta \Delta V_a(\Omega_a)} \\
&= 2 \sum_{b=s,p} \int d\Omega_b \left[\mathcal{F}_{a,b}(\Omega_a; \Omega_b; D) - \frac{\int d\Omega_s \int d\Omega'_s \mathcal{F}_{s,b}(\Omega_s; \Omega_b; D) \mathcal{F}_{s,a}(\Omega'_s; \Omega_a; D)}{\int d\Omega_s \int d\Omega'_s \mathcal{F}_{s,s}(\Omega_s; \Omega'_s; D)} \right] \Delta V_b(\Omega_b). \quad (18)
\end{aligned}$$

Since the above equation must be satisfied for all D and the distance dependence cannot be factored out of the integral, the function in square brackets can take on nearly any value at each point in the integration domain. This leads to the solution for the above integral equation $\Delta V_a(\Omega_a) = 0$ for which it is easy to verify the $F_{\text{sp}}(V_0 = V_{\text{min}}) = 0$. Since this particular choice for the fluctuating potentials gives the extremum for the electrostatic force, any spatial variation of the potentials on the surfaces leads to a nonvanishing patch force. This proves that it is impossible to nullify the electrostatic force by an externally applied potential when patches are present.

D. Insights on the spatial dependence of the minimizing potential from the PFA

Before discussing the results of our numerical simulations, we would like to give some theoretical arguments related to the conditions under which the minimizing potential depends on distance and to what one can infer about patches in the cases where the minimizing potential is distance independent. To begin let us explain the reasons why an externally applied potential is necessary.

In Casimir force experiments there exists an intrinsic potential difference between the samples, the contact potential, V_{con} , which is an average surface potential difference whose physical origin is the electrical connections between the two bodies, differences in work function between the samples, and the presence of patches. In the following considerations we neglect the effects from connecting wires, solder joints, etc., and focus entirely on the contact potential difference arising from work function differences and patches. The contact potential leads to electrostatic forces between the bodies which can dominate over the desired Casimir force signal. By applying an appropriate bias voltage (the minimizing potential) the additional force arising from V_{con} can be nullified. Thus, we can understand the nature of the minimizing potential via its direct relationship to V_{con} . We should emphasize that this bias voltage does not nullify the total electrostatic force, which has components arising from fluctuating patch voltages that are not accounted for in V_{con} .

Our goal now is to try to understand the spatial dependence of the contact potential. To do this we lay out two ideas; the first quantifies the electrostatic sphere-plane force via an effective area of interaction, and the second relates the contact potential to a weighted average of patch voltages. To begin, consider two patchy surfaces interacting within the PFA limit, where the sphere is treated as a large but finite plane. In distinction to the case of two infinite planes the sphere-plane force can be characterized by an effective area of interaction. This is not surprising given that the sphere

has a finite cross section. Within the PFA we can estimate this effective area of interaction by equating the sphere-plane force to the product of the plane-plane pressure and the effective area of interaction, $F_{\text{sp}} = P_{\text{pp}} A_{\text{eff}}$, where F_{sp} is the sphere-plane force and P_{pp} is the plane-plane electrostatic pressure. In the PFA limit the sphere-plane force can be approximated by the plane-plane energy per area E_{pp} , $F_{\text{sp}} \approx 2\pi R E_{\text{pp}}$. By noting that $E_{\text{pp}} \sim D P_{\text{pp}}$ we can solve for the effective area of interaction giving

$$A_{\text{eff}} \sim 2\pi R D. \quad (19)$$

Now we connect the idea of an effective area of interaction with the contact potential. To do so we assume that each of the bodies are polycrystalline structures for which the work function varies above the surface due to the different local grain crystallographic orientation. Given the variation of the potential over the surface we roughly identify the contact potential with the average work function difference between the samples observed within the effective area. Thus, we can write the contact potential formally as

$$V_{\text{con}} \sim \sum_{i,j}^N V_{ij} w_{ij}, \quad (20)$$

where the indices i and j are used to label the patches on the surfaces, N is the number of patches within the effective area, and w_{ij} is a normalized weight which is meant to roughly account for the fact that patches far from the point of the sphere and plane's nearest approach should contribute less to the value of the contact potential.

In order to make these assertions more precise we derive an expression for the minimizing potential (which equals the contact potential) within the PFA limit. We should stress that this analysis only roughly characterizes the spatial variation of the minimizing potential and is used here to gain physical insight.

Our starting point is the expression for the sphere-plane force found in Ref. [19]:

$$F_{\text{sp}} \approx \frac{\varepsilon_0}{2} \int_0^{2\pi} d\phi \int_0^R d\rho \rho \frac{[V_0 - V(\Omega_p)]^2}{(D + \rho^2/2R)^2}, \quad (21)$$

where $V(\Omega_p)$ is the spatially varying potential difference between the two plates, measured at the the polar coordinate on the plane described by Ω_p [note that $V(\Omega_p)$ should not be confused with the patch potential on the plane, $V_p(\Omega_p)$]. By using Eq. (15) we can compute the minimizing potential [this equation also appears in Ref. [19] see Eq. (22)]. After replacing $V(\Omega_p)$ with its average value and its fluctuating component,

i.e., $V(\Omega_p) = \bar{V} + \Delta V(\Omega_p)$, we find

$$V_{\min} = \bar{V} + \frac{\int_0^{2\pi} d\phi \int_0^R d\rho \rho \frac{\Delta V(\Omega_p)}{(D+\rho^2/2R)^2}}{\int_0^{2\pi} d\phi \int_0^R d\rho \rho \frac{1}{(D+\rho^2/2R)^2}}. \quad (22)$$

In order to proceed we assume that $\Delta V(\Omega_p)$ is a piecewise constant function, and we prescribe the geometry of the patches. The simplest choice for the patch layout is to break each surface into rings centered at the point of closest approach and then to divide each annulus into several pieces [see Fig. 2(c)]. Adopting this prescription, evaluating the integral in the denominator above, and using the fact that $D \ll R$, we can write the minimizing potential as

$$V_{\min} = \bar{V} + \sum_{i=1}^M \sum_{j=1}^{K(i)} \int_{\phi_{j-1(i)}}^{\phi_{j(i)}} \frac{d\phi}{2\pi} \int_{\rho_{i-1}}^{\rho_i} \frac{d\rho}{R} \frac{\rho D \Delta V_{ij}}{(D + \rho^2/2R)^2}. \quad (23)$$

Above, the indices i and j label each of the patches, i denoting the ring and j denoting the angular sector. The term ΔV_{ij} gives the fluctuating part of the potential which is constant within the boundary of each patch. The total number of rings is given by M , $K(i)$ is the number patches in the i th ring, the coordinates $\phi_j(i)$ denote the angular boundaries of the patch sectors in the i th ring, and ρ_i denotes the outer radius of the i th ring. For simplicity we consider the case where $\rho_i = ir_{\text{ave}}$ and divide the i th ring into $2i - 1$ equal pieces. In this way each patch has a fixed area, πr_{ave}^2 , and our expression above for the minimizing potential can be simplified. This discretization of the surface certainly does not correspond precisely with a realistic distribution of patches on the sample surfaces and is not unique either. Despite this limitation we believe that this crude approximation can provide some insights into the behavior of the minimizing potential.

After applying this discretization we find the simplified expression for the minimizing potential:

$$V_{\min} = \bar{V} + \sum_{i=1}^M \sum_{j=1}^{2i-1} \frac{\frac{r_{\text{ave}}^2}{2DR} \Delta V_{ij}}{\left(1 + (i-1)^2 \frac{r_{\text{ave}}^2}{2DR}\right) \left(1 + i^2 \frac{r_{\text{ave}}^2}{2DR}\right)}, \quad (24)$$

where $M = R/r_{\text{ave}}$ (since M must be an integer one should take M to be the floor of R/r_{ave} in numerical computations). Since the minimizing and contact potentials are equal we can use Eq. (24) with Eq. (20) to obtain an expression for the weights:

$$w_{ij} = \frac{\frac{r_{\text{ave}}^2}{2DR}}{\left(1 + (i-1)^2 \frac{r_{\text{ave}}^2}{2DR}\right) \left(1 + i^2 \frac{r_{\text{ave}}^2}{2DR}\right)}. \quad (25)$$

It is interesting to note that these weights are parametrized by $r_{\text{ave}}^2/2DR$, which is the ratio of the patch area to the effective area of interaction. One can see that when many patches fit inside the effective area of interaction, i.e., $r_{\text{ave}}^2/2DR \ll 1$, then $w_{ij} \propto r_{\text{ave}}^2/2DR$ for small i (innermost rings), and becomes successively smaller for larger rings. At the outermost ring $w_{ij} \approx \frac{r_{\text{ave}}^2}{2DR} \frac{4D^2}{R^2}$. Therefore, in this case, all rings contribute to the average but their influence is suppressed for large i as $1/i^4$. In comparison, when the patch area is much larger than the effective area of interaction, i.e., $r_{\text{ave}}^2/2DR \gg 1$, the weight for the innermost ring is close to 1, and the weights for all other rings are strongly suppressed, roughly proportional

to $2DR/r_{\text{ave}}^2$. Therefore, in the large patch scenario only the patch located at the position of closest approach contributes to the contact potential.

So far we have considered the contact potential for a fixed microrealization of patches, meaning that the voltages and geometry of each patch have been assigned and fixed. This is the case one would encounter in an experiment. At this stage our calculation cannot proceed without a direct knowledge of the patch layout on the surfaces. However, based on the simple arguments made above it is not hard to make some qualitative statements about the expected sample-to-sample fluctuations of the contact potential as a function of separation. These arguments would apply to statistics on an ensemble of minimizing potential measurements performed with samples fabricated in the same way. Since the contact potential is roughly an average, the more patches which contribute to the average the more suppressed will be the sample-to-sample fluctuations. This can be roughly understood because the uncertainty in an average value scales like $1/\sqrt{N}$, where N is the number of data points used to compute the average. Therefore, a small patch size will lead to small minimizing potential fluctuations because more patches will determine the contact potential. The converse is true for large patches. For the same reasons large separations will lead to suppressed minimizing potential fluctuations since the effective area of interaction grows with separation. Likewise, at small separations as the ratio $r_{\text{ave}}^2/2DR$ becomes large one should expect large sample-to-sample fluctuations of the contact potential.

We can make these qualitative assertions more concrete by making statistical assumptions about the patch voltages. If each of the potentials is assumed to be assigned randomly and statistically independently of one another, and with the same variance, then the expected variation of the sum on j takes the form $\sum_{j=1}^{2i-1} \Delta V_{ij} = \pm \sqrt{2i-1} V_{\text{rms}}$, where V_{rms} characterizes the expected rms fluctuations of the assigned potential for a single patch. This leads to the expected range of minimizing potential values given by

$$\bar{V} \pm V_{\text{rms}} \underbrace{\sum_{i=1}^M \frac{\frac{r_{\text{ave}}^2}{2DR} \sqrt{2i-1}}{\left[1 + (i-1)^2 \frac{r_{\text{ave}}^2}{2DR}\right] \left(1 + i^2 \frac{r_{\text{ave}}^2}{2DR}\right)}}_{\sigma_{V_{\min}}(D)}. \quad (26)$$

Thus, in a given experiment, i.e., one microrealization of patches, we would expect the minimizing potential to vary in position within a few $\sigma_{V_{\min}}(D)$ of \bar{V} . The variation is suppressed at large distances because averaging is performed over larger and larger effective areas. However in the case of large patches, $r_{\text{ave}}^2/2DR \gg 1$, the $i = 1$ term in the sum dominates and the expected variation is given roughly by V_{rms} .

Above we have made some rough arguments in order to characterize the expected variation of the contact potential. We should stress that this expected variation will tell us nothing about the minimizing potential in a single experiment: Eq. (26) will not yield a prediction for the minimizing potential as a function of distance. Rather, the arguments above apply to an ensemble of measurements of the minimizing potential for different samples prepared in the same way. The expected fluctuations will only tell us the envelope within which roughly

66% of minimizing potential measurements of various samples will lie.

The above analysis makes it clear that, in principle, the minimizing potential always depends on distance when patches are present. However, when the expected variation of the contact potential is much smaller than the uncertainty in the measurements, the minimizing potential will appear in practice to be independent of distance. This behavior is expected when the typical patch size is much smaller than the effective area of interaction and, as we soon show, can be accompanied by a nonvanishing patch force.

III. NUMERICAL RESULTS

In this section we present our numerical results for the sphere-plane minimizing potential (16) and the residual electrostatic force (17) for various patch sizes.

A. Minimizing potential and electrostatic patch force

To compute the minimizing potential we evaluate Eq. (16) in several steps. First, the sphere and the plane are tessellated (see Fig. 2), and then each patch is independently and randomly assigned a potential from the values 5.15, 5.04, and 5.10 V, corresponding to the work functions of the three principal crystallographic orientations of gold [30]. For each microrealization, defined by a given layout of potentials and patch geometries, we compute the minimizing potential using Eq. (16). Given an ensemble of minimizing potential “measurements” we perform statistics to recover the mean value and the expected variation. For numerical simplicity we keep the geometry of the patch layout fixed in all microrealizations. Another point to acknowledge is that we assume that the average potential for the sphere and the plane are equal, as if they are made from the same material, and therefore $\bar{V}_p = \bar{V}_s$.

The tessellation is performed using a ringlike division of the sphere and the plane as is depicted in Fig. 2(a). The plane

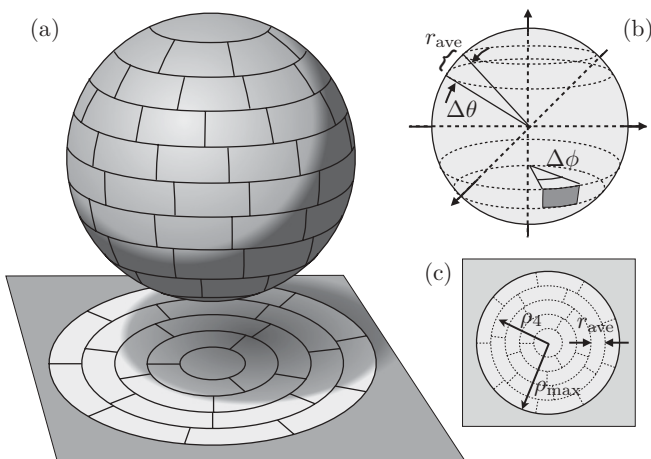


FIG. 2. (a) Illustration of the tessellation used for our simulations. (b) Rings chosen on the sphere. (c) Patch layout on the plane. In the numerics the parameter ρ_{max} is chosen to be larger than $5R$ [although in panel (a) $\rho_{max} \approx R$ for illustration purposes]. For the PFA analysis of the spatial dependence of the minimizing potential both plates are tessellated as is depicted in panel (c).

is divided into annuli in the same manner described above for the PFA treatment of the spatial dependence of the minimizing potential. The outer radius of the i th annulus, ρ_i , is given by ir_{ave} and therefore the width of each annulus is given by r_{ave} . The i th ring is divided into $2i - 1$ equal pieces so that all patches have the same area. In order to manage the computation time we set the patch potentials to the average potential for radii greater than ρ_{max} , which is chosen large enough so that all results converge. As we mentioned in our PFA analysis above, we acknowledge that this type of tessellation of the plane does not correspond with any realistic layout of patches on the plane. We believe, however, that this approximation is sufficient to gain some insight about the patch size dependence of the force. Next, the sphere is tessellated in a similar manner by being divided into a fixed number of latitudinal lines, any neighboring pair subtending polar angle $\Delta\theta$; afterward the lines of longitude dividing a given ring are chosen so that all of the patches have the same area. We chose $\Delta\theta$ to take the value $R\Delta\theta = r_{ave}$. For this particular tessellation the polar angle describing the upper boundary of the i th ring is given by $\theta_i = \pi - \frac{r_{ave}}{R}i$ where we have chosen $i = 0$ to correspond with the polar angle of the “south pole.” With the particular choice we have adopted for the polar angles of the rings we find the number of patches in the i th ring on the sphere is given by $|\text{Floor}[(2R^2/r_{ave}^2)(\cos\theta_{i-1} - \cos\theta_i)]|$.

The numerical results for the minimizing potential are presented in Fig. 3. All of the plots employ the same convention: the solid line denotes the average minimizing potential as a function of distance, and the dashed lines are computed from the standard deviations of all the minimizing potential values at each separation. Thus, by definition, the envelope created by the two dashed lines contains roughly 66% of all minimizing potential measurements. The data points indicated by the various plot markers are the values of the minimizing potential from five random microrealizations. The figure illustrates the spatial dependence of the minimizing potential on patch size. In line with our PFA analysis, as the patch size grows [from Figs. 3(a) to 3(c)] the expected minimizing potential fluctuations are enhanced. Additionally, for each patch size the effective area of interaction decreases as the sphere-plane distance becomes smaller. Thus, the shorter the distance, the fewer the patches which contribute to the average that determines the minimizing potential, and hence the larger are the fluctuations.

To obtain the sphere-plane electrostatic patch force Eq. (14), we employ the tessellation described above (see Fig. 2). Once we have an ensemble of realizations we find the average patch force and its expected fluctuations. The results of our simulations are depicted in Fig. 4. We also compare these numerical results with the patch force computed by performing an average over voltage microrealizations analytically while keeping the patch geometrical layout fixed. To do this we compute the two-point voltage correlation functions on the plates, where we assume that the voltages on each patch are statistically independent, random variables (so-called “quasilocal correlation,” see Eqs. (10)–(12) of Ref. [23]),

$$\langle V_a(\mathbf{x})V_b(\mathbf{x}') \rangle_v = \delta_{ab} V_{rms}^2 \sum_i \Theta_i(\mathbf{x})\Theta_i(\mathbf{x}'), \quad (27)$$

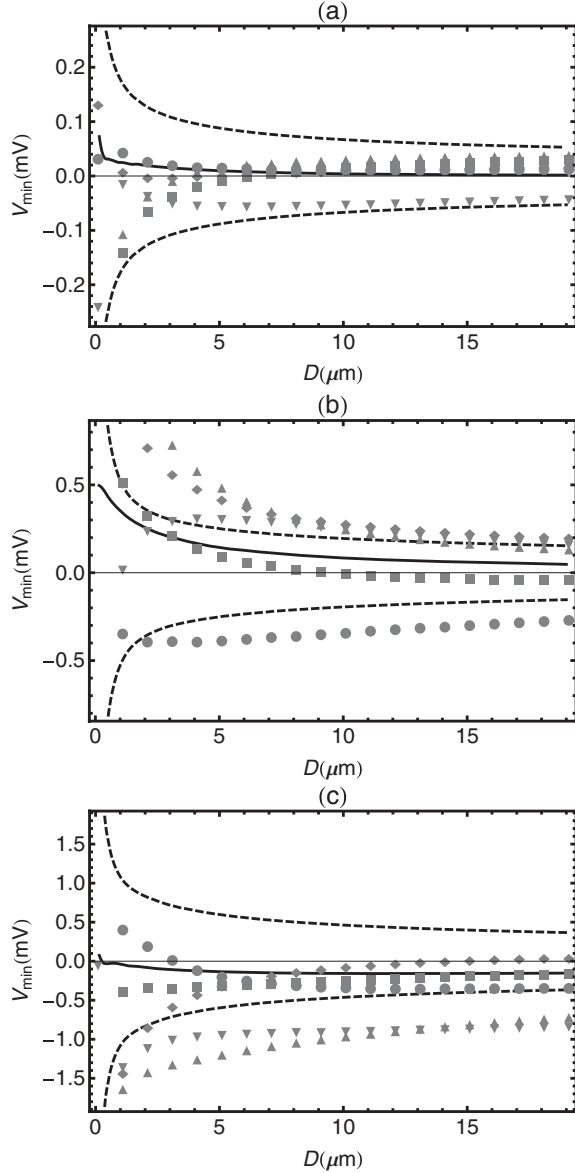


FIG. 3. Minimizing potential (16) as a function of distance for various patch sizes: (a) 100 nm, (b) 300 nm, and (c) 600 nm. The solid curve is the average minimizing potential computed from 400 microrealizations. The dashed curves enclose the range of expected fluctuations computed from the standard deviation of all minimizing potential values at a fixed distance. The data points denote the minimizing potential for five random microrealizations. The radius of the sphere is $R = 150 \mu\text{m}$ and the average potentials of the sphere, \bar{V}_s , and the plane, \bar{V}_p , are set equal.

where the function $\Theta_i(\mathbf{x})$ is 1 for points \mathbf{x} within the i th patch and 0 otherwise. Using this equation in Eq. (14) we compute the ensemble-averaged patch force $\langle F_{\text{sp}} \rangle_v$. In Fig. (4) we compare the exact numerics with the patch force computed via the voltage correlation method. As seen in the figure, the agreement between the two is excellent. In the inset we compare the residual electrostatic force (17) with the above patch force (14). The two forces are very similar, illustrating that the electrostatic calibration does not nullify the patch force.

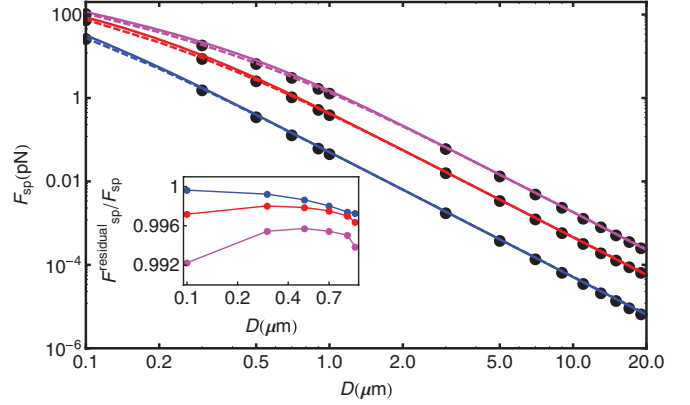


FIG. 4. (Color online) Sphere-plane electrostatic patch force (14) as a function of separation for different patch sizes, from top to bottom: 600 nm (magenta), 300 nm (red), and 100 nm (blue). The data points are the average patch force, the error bars are not visible at the scale shown, the dashed lines are the patch force computed with the voltage correlation method, and the solid lines denote the patch force computed using the PFA and averaging over patch layouts and voltages (as in Ref. [23]). Inset: Ratio of the residual force (17) to the patch force (14) as a function of separation for different patch sizes. From bottom to top: 600 nm (magenta), 300 nm (red), and 100 nm (blue). The radius of the sphere is $R = 150 \mu\text{m}$, the average potentials of the sphere, \bar{V}_s , and the plane, \bar{V}_p , are set equal, and the rms potential is $V_{\text{rms}} = 45 \text{ mV}$.

B. Comparison with the PFA

Here we compare our computations of the sphere-plane patch force using the exact expression with the results of a previous paper [23] that used the PFA and treated the product of surface voltages using an ensemble-averaging scheme.

As discussed in Sec. IID, the PFA to the sphere-plane electrostatic force is

$$F_{\text{sp}}^{\text{PFA}} = 2\pi R E_{\text{pp}}, \quad (28)$$

where E_{pp} is the plane-plane electrostatic interaction energy per unit area. This is given by

$$E_{\text{pp}} = -\frac{\epsilon_0}{2A} \int d^2\mathbf{x} \int d^2\mathbf{x}' \int \frac{d^2\mathbf{k}}{4\pi^2} e^{i\mathbf{k}\cdot(\mathbf{x}-\mathbf{x}')} k \times \left\{ \frac{2}{e^{2kD} - 1} [V_1(\mathbf{x})V_1(\mathbf{x}') + V_2(\mathbf{x})V_2(\mathbf{x}')] - \frac{1}{\sinh kD} [V_2(\mathbf{x})V_1(\mathbf{x}') + V_1(\mathbf{x})V_2(\mathbf{x}')] \right\}, \quad (29)$$

where A is the area of the plates and V_i is the potential of the i th plate. Using the same tessellation as before [as in Fig. 2(c)] we could compute this plane-plane energy per unit area and the PFA equivalent sphere-plane force, both for individual microrealizations and when an ensemble averaging is performed over the surface voltage layout. If arbitrary tessellations could be generated numerically we could also include a second level of ensemble averaging over patch geometries. For simplicity we compare our exact numerics, which uses a fixed patch layout, with the patch force computed in Ref. [23], which used the PFA and an ensemble average over both patch voltages and geometries.

The solid lines in the main Fig. 4 correspond with the patch force computed using the PFA and the two-point voltage correlation function $\langle V(\mathbf{x})V(\mathbf{x}') \rangle$ computed with the quasilocal correlation model (see Eqs. (2) and (14) of Ref. [23]), with the further assumption that the distribution of patch sizes $\Pi(\ell)$ defined in Eq. (13) of Ref. [23] is given by a δ function (i.e., single patch size). As can be seen, the results of Ref. [23] (solid lines) are in very good agreement with the exact patch force computation (using the particular tessellation employed in this paper, see Fig. 2), depicted as dashed lines. The small differences between them are attributed to the geometrical averaging done in the latter method. Indeed, at larger distances the shape of the individual patches becomes less important, and hence the results of the two calculations converge to each other (note that this is only true because, for the distances shown, we are still well within the regime of validity for the PFA). In addition, our results indicate that the patch force is remarkably robust with regard to the details of the geometry of the patches.

IV. CONCLUSIONS

In this paper we derived the exact expression for the sphere-plane electrostatic potential, interaction energy, and force for patchy boundary conditions. With knowledge of the potentials on the sample surfaces used in Casimir force experiments in the sphere-plane geometry, to be measured by dedicated experiments, these expressions can be used to exactly quantify the sphere-plane force due to patch potentials.

As an added benefit of the exact solution we were able to derive an exact formula for the minimizing potential used to calibrate many Casimir force experiments. We found that when patches are present the minimizing potential always depends on position. However, the magnitude of the spatial fluctuations is controlled by the ratio of the typical patch size to the effective area of interaction. In the limit where this ratio is small the expected spatial modulation of the minimizing potential is suppressed, and provided that the expected variation is smaller than the experimental uncertainty it will appear to be independent of position. We verified this behavior numerically. Using proximity force arguments and numerical computations we were also able to show the following qualitative behavior: the typical fluctuations of the minimizing potential decay as a function of sphere-plane separation and correlate with the typical patch size. Our PFA analysis suggests that both of these observations can be understood in terms of a weighted average over the patches on both surfaces. When many patches contribute to the average (by having comparable weights) the expected fluctuations of the minimizing potential are suppressed. This happens when many patches fit within the effective area of interaction. In contrast, the expected fluctuations are greatly enhanced when the typical patch area is comparable to the effective area of interaction, as the patch at the point of nearest approach dominates the weighted average.

We also derived an explicit formula for the residual electrostatic force (17) that persists in Casimir force measurements after an electrostatic calibration has been performed. By analyzing the residual electrostatic force we proved that the electrostatic interaction cannot be nullified by an applied field unless there are no patches. This behavior was also verified in our simulations.

Finally we compared our exact results with previous work [23] that used the PFA in conjunction with an averaging scheme for the surface voltages and patch geometries to evaluate the sphere-plane patch force. Despite the limited nature of the tessellations used in our simulations of the exact patch force, we found a remarkable agreement between the two calculations. This suggests that the sphere-plane patch force is robust with regard to the details of the geometrical patch layout.

ACKNOWLEDGMENTS

We would like to acknowledge fruitful discussions with Ricardo Decca, Francesco Intravaia, Woo-Joong Kim, Astrid Lambrecht, Steve Lamoreaux, Paulo Maia Neto, Clive Speake, Alex Sushkov, and Andrew Sykes.

APPENDIX A: ELECTROSTATIC SELF-ENERGIES

In this Appendix we compute the large separation limit of the electrostatic sphere-plane energy (11) in order to identify the self-energies of the sphere and the plane in bispherical coordinates and show that they correspond to the well-known self-energies of each of these objects.

We start with the computation of the self-energy for the sphere. First, we briefly recall the derivation of its electrostatic self-energy in spherical coordinates. The electrostatic potential for an isolated sphere of radius R with surface patch potentials $V_s(\Omega) = V_s(\theta, \phi)$ is given by the known solution of the Laplace equation in spherical coordinates,

$$V(\mathbf{x}) = \sum_{\ell=0}^{\infty} \sum_{m=-\ell}^{\ell} \frac{\lambda_{\ell}}{2\pi} (-1)^m \left(\frac{R}{r}\right)^{\ell+1} \int d\Omega'_s e^{im(\phi-\phi')} \times P_{\ell}^m(\cos\theta) P_{\ell}^{-m}(\cos\theta') V_s(\Omega'_s). \quad (\text{A1})$$

Similar to the procedure used in the main text, we use the Gauss divergence theorem to express the sphere self-energy as

$$E_s^{\text{self}} = -\frac{\epsilon_o}{2} \int_S d\mathbf{a} \cdot \nabla V_s(\Omega) \hat{\mathbf{r}} \left. \frac{\partial}{\partial r} V(\mathbf{x}) \right|_{r=R}, \quad (\text{A2})$$

where the integration is over the sphere's surface. In this way we obtain the known electrostatic self-energy of the sphere in spherical coordinates

$$E_s^{\text{self}} = \frac{\epsilon_o}{2} R \sum_{\ell=0}^{\infty} \sum_{m=-\ell}^{\ell} \frac{\lambda_{\ell}(\lambda_{\ell} + 1/2)}{2\pi} (-1)^m \int d\Omega_s \int d\Omega'_s \times e^{im(\phi-\phi')} P_{\ell}^m(\cos\theta) P_{\ell}^{-m}(\cos\theta') V_s(\Omega_s) V_s(\Omega'_s), \quad (\text{A3})$$

where we used that $\lambda_{\ell} = \ell + 1/2$.

Next we show that by taking the large distance limit in Eq. (11), the piece which is a quadratic function of the sphere's potential gives exactly this result for the sphere's self-energy. When $D \rightarrow \infty$, or equivalently when $\Lambda \rightarrow \infty$, we get from Eq. (11)

$$E_s^{\text{self}} = \lim_{\Lambda \rightarrow \infty} \frac{\epsilon_o}{2} R \sum_{\ell=0}^{\infty} \sum_{k=-\ell}^{\ell} \frac{\lambda_{\ell}(\lambda_{\ell} + 1/2)}{2\pi} (-1)^k \int d\Omega \int d\Omega' \times e^{ik(\phi-\phi')} P_{\ell}^k(\cos\xi) P_{\ell}^{-k}(\cos\xi') V_s(\Omega) V_s(\Omega'). \quad (\text{A4})$$

We use the following identities that relate bispherical coordinates with spherical coordinates centered on the sphere:

$$\cos \xi = \frac{1 + \cosh \Lambda \cos \theta}{\cosh \Lambda + \cos \theta}, \quad (\text{A5})$$

$$\sin \xi = \frac{\sinh \Lambda \sin \theta}{\cosh \Lambda + \cos \theta}, \quad (\text{A6})$$

$$\sin \xi d\xi = \frac{\sinh^2 \Lambda}{(\cosh \Lambda + \cos \theta)^2} \sin \theta d\theta, \quad (\text{A7})$$

$$\frac{1}{(\cosh \Lambda - \cos \xi)^n} = \frac{(\cosh \Lambda + \cos \theta)^n}{\sinh^{2n} \Lambda}. \quad (\text{A8})$$

For $\Lambda \rightarrow \infty$ we obtain $\cos \xi \rightarrow \cos \theta$, $d\Omega \rightarrow d\Omega_s$, and therefore the sphere self-energy in bispherical coordinates (A4) is identical to that in spherical coordinates (A3), as expected.

We now consider the self-energy for the plane. The electrostatic potential for an isolated plane located at $z = 0$ having surface patch potentials $V_p(\Omega) = V_p(\mathbf{r})$ [$\mathbf{r} = (x, y)$] is

$$V(\mathbf{x}) = \int \frac{d^2 \mathbf{k}}{(2\pi)^2} e^{i\mathbf{k} \cdot \mathbf{r}} e^{-kz} V_p(\mathbf{k}), \quad (\text{A9})$$

where $V_p(\mathbf{k})$ is the two-dimensional Fourier transform of the patchy potential. The self-energy is

$$\begin{aligned} E_p^{\text{self}} &= \frac{\varepsilon_o}{2} \int d^2 \mathbf{x} V_p(\mathbf{x}) \left. \frac{\partial}{\partial z} V(\mathbf{x}) \right|_{z=0} \\ &= \frac{\varepsilon_o}{2} \int d^2 \mathbf{r} \int d^2 \mathbf{r}' V_p(\mathbf{r}) f(\mathbf{r} - \mathbf{r}') V_p(\mathbf{r}'), \end{aligned} \quad (\text{A10})$$

where $f(\mathbf{r} - \mathbf{r}') = (2\pi)^{-2} \int d^2 \mathbf{k} |\mathbf{k}| e^{i\mathbf{k} \cdot (\mathbf{r} - \mathbf{r}')} = -(2\pi)^{-1} |\mathbf{r} - \mathbf{r}'|^{-3}$.

As for the case of the self-energy for the sphere, we take the $D \rightarrow \infty$ limit (or, equivalently, the $a \rightarrow \infty$ limit) of Eq. (11) and focus on the term that depends on the plane. We get

$$\begin{aligned} E_p^{\text{self}} &= \frac{\varepsilon_o}{2} a \sum_{\ell=0}^{\infty} \sum_{k=-\ell}^{\ell} \frac{\lambda_{\ell}^2}{2\pi} (-1)^k \int d\Omega \int d\Omega' \\ &\times \frac{e^{ik(\phi-\phi')} P_{\ell}^k(\cos \xi) P_{\ell}^{-k}(\cos \xi') V_p(\Omega) V_p(\Omega')}{\sqrt{1 - \cos \xi} \sqrt{1 - \cos \xi'}}. \end{aligned} \quad (\text{A11})$$

In order to show that this is identical to (A10) we first perform the summation over k in Eq. (A11). For this we use the addition theorem of Legendre polynomials, $\sum_{k=-\ell}^{\ell} (-1)^k e^{ik(\phi-\phi')} P_{\ell}^k(\cos \xi) P_{\ell}^{-k}(\cos \xi') = P_{\ell}(\cos \gamma)$, where

$$\cos \gamma = \cos \xi \cos \xi' + \sin \xi \sin \xi' \cos(\phi - \phi'). \quad (\text{A12})$$

In the resulting equation we then change the coordinate system from bispherical coordinates to polar coordinates on the plane ($\eta = 0$), centered at the point of closest approach between the sphere and the plane, i.e., right below the sphere. The polar coordinate ρ relates to the bispherical coordinate ξ through $\rho = a \cot \xi/2$. The following identities are useful to relate both coordinate systems:

$$\cos \xi = \frac{(\rho/a)^2 - 1}{(\rho/a)^2 + 1}, \quad (\text{A13})$$

$$\sin \xi = \frac{2(\rho/a)}{(\rho/a)^2 + 1}, \quad (\text{A14})$$

$$\frac{\sin \xi d\xi}{\sqrt{1 - \cos \xi}} = -\frac{2\sqrt{2}\rho d\rho}{a^2[1 + (\rho/a)^2]^{3/2}}. \quad (\text{A15})$$

Then Eq. (A11) takes the form

$$\begin{aligned} E_p^{\text{self}} &= \lim_{a \rightarrow \infty} \frac{2\varepsilon_o}{\pi a^3} \int d\Omega_p \int d\Omega'_p V_p(\Omega_p) V_p(\Omega'_p) \\ &\times \sum_{\ell=0}^{\infty} \lambda_{\ell}^2 P_{\ell}(\cos \gamma), \end{aligned} \quad (\text{A16})$$

where $\Omega_p = (\rho, \phi)$ are the polar coordinates on the plane and $d\Omega_p$ is the corresponding measure. The above summation can be evaluated using the generating function of Legendre polynomials, which verifies

$$S(t, u) \equiv \sum_{\ell=0}^{\infty} t^{\ell} P_{\ell}(u) = \frac{1}{\sqrt{1 - 2tu + t^2}}. \quad (\text{A17})$$

Recalling that $\lambda_{\ell} = \ell + 1/2$, we obtain

$$\begin{aligned} \sum_{\ell=0}^{\infty} \lambda_{\ell}^2 t^{\ell} P_{\ell}(u) &= \left(t \frac{\partial}{\partial t} - t \frac{\partial}{\partial t} + t \frac{\partial}{\partial t} + \frac{1}{4} \right) S(t, u) \\ &= \frac{1 - 10t^2 + t^4 + 4t(1 + t^2)u}{4(1 + t^2 - 2tu)^{5/2}} \\ &\equiv \mathcal{G}(t, u). \end{aligned} \quad (\text{A18})$$

Setting $t = 1$ we derive the identity $\sum_{\ell=0}^{\infty} \lambda_{\ell}^2 P_{\ell}(\cos \gamma) = -[2(1 - \cos \gamma)]^{-3/2}$. Using Eqs. (A13) and (A14) in the definition of $\cos \gamma$ and taking the $a \rightarrow \infty$ limit we obtain $1 - \cos \gamma \approx 2|\mathbf{r} - \mathbf{r}'|/a^2$. Hence Eq. (A16) is equal to

$$E_p^{\text{self}} = -\frac{\varepsilon_o}{4\pi} \int d^2 \mathbf{r} \int d^2 \mathbf{r}' V_p(\mathbf{r}) |\mathbf{r} - \mathbf{r}'|^{-3} V_p(\mathbf{r}'), \quad (\text{A19})$$

which is exactly the plane self-energy in polar coordinates (A10), as it should.

APPENDIX B: DERIVATION AND EXPRESSION OF SPHERE-PLANE ENERGY KERNELS

In this Appendix we give the derivation of the kernels appearing in Eq. (13). We first write the energy (11) in a compact form, $E_{\text{sp}} = E_{\text{sp}}^{\text{s,s}} + E_{\text{sp}}^{\text{s,p}} + E_{\text{sp}}^{\text{p,s}} + E_{\text{sp}}^{\text{p,p}}$, where the superscripts denote which surface potentials contribute to each term. For example, let us consider the $E_{\text{sp}}^{\text{s,s}}$ term:

$$\begin{aligned} E_{\text{sp}}^{\text{s,s}} &= \frac{\varepsilon_o}{2} R \sinh \Lambda \sum_{\ell=0}^{\infty} \sum_{k=-\ell}^{\ell} \frac{\lambda_{\ell}}{2\pi} (-1)^k \\ &\times \int d\Omega \int d\Omega' e^{ik(\phi-\phi')} P_{\ell}^k(\cos \xi) P_{\ell}^{-k}(\cos \xi') \\ &\times \frac{V_s(\Omega) V_s(\Omega')}{\sqrt{\cosh \Lambda - \cos \xi} \sqrt{\cosh \Lambda - \cos \xi'}} \\ &\times \left(\lambda_{\ell} \coth \lambda_{\ell} \Lambda + \frac{\sinh L}{2(\cosh \Lambda - \cos \xi)} \right). \end{aligned} \quad (\text{B1})$$

In order to simplify the above expression we first notice that the second term in the parentheses is independent of ℓ , which allows us to use the completeness relation for the associated

Legendre polynomials,

$$\sum_{\ell=0}^{\infty} \sum_{k=-\ell}^{\ell} \frac{\lambda_{\ell}}{2\pi} (-1)^k e^{ik(\phi-\phi')} P_{\ell}^k(\cos \xi) P_{\ell}^{-k}(\cos \xi') = \delta(\phi - \phi') \delta(\cos \xi - \cos \xi'), \quad (\text{B2})$$

and perform the Ω integral. We also notice that the first term in the parentheses can be written as $\coth \lambda_{\ell} \Lambda = 2 \sum_{n=0}^{\infty} e^{-2\lambda_{\ell} \Lambda n}$, where the prime in the summation symbol indicates that the $n = 0$ term has to be taken with half weight. By using the completeness relation, Eq. (B2), the addition theorem for Legendre polynomials, and the identity equation, Eq. (C2), we can express $E_{\text{sp}}^{\text{s,s}}$ as

$$E_{\text{sp}}^{\text{s,s}} = \frac{\varepsilon_0 R}{4} \int d\Omega \frac{\sinh^2 \Lambda V_s^2(\Omega)}{(\cosh \Lambda - \cos \xi)^2} + \frac{\varepsilon_0}{2\pi} \sum_{n=0}^{\infty} e^{-\Lambda n} \int d\Omega \int d\Omega' \frac{a V_s(\Omega) V_s(\Omega') \mathcal{G}(e^{-2\Lambda n}, \cos \gamma)}{\sqrt{\cosh \Lambda - \cos \xi} \sqrt{\cosh \Lambda - \cos \xi'}}, \quad (\text{B3})$$

where we have introduced the function $\mathcal{G}(t, u)$, defined in Eq. (C2). Using the identities in Appendix A, which relate bispherical and spherical coordinates, we obtain

$$E_{\text{sp}}^{\text{s,s}} = \frac{\varepsilon_0 R}{4} \int d\Omega_s V_s^2(\Omega_s) + \frac{\varepsilon_0}{2\pi} \sum_{n=0}^{\infty} e^{-\Lambda n} \int d\Omega_s \int d\Omega_{s'} \frac{R \sinh^3 \Lambda V_s(\Omega_s) V_s(\Omega_{s'}) \mathcal{G}(e^{-2\Lambda n}, \cos \gamma^{\text{s,s}})}{(\cosh \Lambda + \cos \theta)^{3/2} (\cosh \Lambda + \cos \theta')^{3/2}}, \quad (\text{B4})$$

where $\cos \gamma^{\text{s,s}}$ is given by Eq. (A12) for the two bispherical coordinates (ξ, ϕ) and (ξ', ϕ') written in terms of spherical coordinates, namely,

$$\cos \gamma^{\text{s,s}} = \frac{(1 + \cosh \Lambda \cos \theta)(1 + \cosh \Lambda \cos \theta') + \sinh^2 \Lambda \sin \theta \sin \theta' \cos(\phi - \phi')}{(\cosh \Lambda + \cos \theta)(\cosh \Lambda + \cos \theta')}. \quad (\text{B5})$$

The same kind of calculations can be performed for the other terms, $E_{\text{sp}}^{\text{s,p}}$, $E_{\text{sp}}^{\text{p,s}}$, and $E_{\text{sp}}^{\text{p,p}}$, in the energy equation, Eq. (11). In this way we derive the energy kernels that appear in (13):

$$\mathcal{E}_{\text{s,s}}(\Omega_s; \Omega'_s; D) = \underbrace{\frac{\varepsilon_0 R}{4} \delta(\phi - \phi') \delta(\cos \theta - \cos \theta')}_{\text{self-energy}} + \frac{\varepsilon_0}{4\pi} R \lim_{\Lambda \rightarrow \infty} \mathcal{G}(1, \cos \gamma^{\text{s,s}}) + \frac{\varepsilon_0}{2\pi} \sum_{n=1}^{\infty} \frac{R \sinh^3 \Lambda e^{-\Lambda n} \mathcal{G}(e^{-2\Lambda n}, \cos \gamma^{\text{s,s}})}{(\cosh \Lambda + \cos \theta)^{3/2} (\cosh \Lambda + \cos \theta')^{3/2}}, \quad (\text{B6})$$

$$\mathcal{E}_{\text{s,p}}(\Omega_s; \Omega_p; D) = \mathcal{E}_{\text{p,s}}(\Omega_s; \Omega_p; D) = -\frac{\sqrt{2}\varepsilon_0}{\pi} \sum_{n=0}^{\infty} \frac{R^2 \sinh^2 \Lambda e^{-\lambda_n \Lambda} \mathcal{G}(e^{-2\lambda_n \Lambda}, \cos \gamma^{\text{s,p}})}{(\cosh \Lambda + \cos \theta)^{3/2} (R^2 \sinh^2 \Lambda + \rho^2)^{3/2}}, \quad (\text{B7})$$

$$\mathcal{E}_{\text{p,p}}(\Omega_p; \Omega'_p; D) = \underbrace{-\frac{\varepsilon_0}{4\pi} \frac{1}{|\mathbf{x} - \mathbf{x}'|^3}}_{\text{self-energy}} + \frac{4\varepsilon_0}{\pi} \sum_{n=1}^{\infty} \frac{R^3 \sinh^3 \Lambda e^{-\Lambda n} \mathcal{G}(e^{-2\Lambda n}, \cos \gamma^{\text{p,p}})}{(R^2 \sinh^2 \Lambda + \rho^2)^{3/2} (R^2 \sinh^2 \Lambda + \rho'^2)^{3/2}}. \quad (\text{B8})$$

The dependency of these kernels on the sphere-plane separation D is encoded in Λ , which we recall depends on D as $\cosh \Lambda = 1 + D/R$. The functions $\cos \gamma^{\text{s,p}}$ and $\cos \gamma^{\text{p,p}}$ are obtained by expressing Eq. (A12) in terms of the corresponding spherical or polar coordinates:

$$\cos \gamma^{\text{s,p}} = \frac{\rho^2 - R^2 \sinh^2 \Lambda}{\rho^2 + R^2 \sinh^2 \Lambda} \frac{1 + \cosh \Lambda \cos \theta}{\cosh \Lambda + \cos \theta} + \frac{2R\rho \sinh \Lambda}{\rho^2 + R^2 \sinh^2 \Lambda} \frac{\sinh \Lambda \sin \theta}{\cosh \Lambda + \cos \theta} \cos(\phi - \phi'), \quad (\text{B9})$$

$$\cos \gamma^{\text{p,p}} = \frac{(\rho^2 - R^2 \sinh^2 \Lambda)(\rho'^2 - R^2 \sinh^2 \Lambda) + 4R^2 \rho \rho' \sinh^2 \Lambda \cos(\phi - \phi')}{(\rho^2 + R^2 \sinh^2 \Lambda)(\rho'^2 + R^2 \sinh^2 \Lambda)}. \quad (\text{B10})$$

The first two terms in Eq. (B6) and the first term in Eq. (B8) correspond to the self-energies of the sphere and the plane, respectively, already derived in Appendix A. These should be removed from the energy kernels when computing the interaction energy or force.

APPENDIX C: EQUIPOTENTIAL CASE

In this Appendix we show how to obtain from our general formula (11) the electrostatic energy when both the sphere and the plane are equipotentials. First we consider the component of the energy depending quadratically on the sphere's potential:

$$E_{\text{eq-p}}^{\text{s,s}} = \frac{\varepsilon_0}{2} V_s^2 \sum_{\ell=0}^{\infty} \sum_{k=-\ell}^{\ell} \frac{\lambda_{\ell}}{2\pi} (-1)^k \int d\Omega \int d\Omega' e^{-ik(\phi-\phi')} P_{\ell}^k(\cos \xi) P_{\ell}^{-k}(\cos \xi') \times \left\{ \frac{a}{\sqrt{\cosh \Lambda - \cos \xi}} \left[\frac{1}{\sqrt{\cosh \Lambda - \cos \xi'}} \left(\lambda_{\ell} \coth \lambda_{\ell} \Lambda + \frac{\sinh \Lambda}{2(\cosh \Lambda - \cos \xi)} \right) \right] \right\}. \quad (\text{C1})$$

The ϕ integrals can be done directly giving Kronecker δ 's which collapse the sum on k , and the integrals over ξ can be done after using the identity $\frac{1}{\sqrt{\cosh \Lambda - x}} = \sqrt{2}e^{-\Lambda/2} \sum_{n=0}^{\infty} P_n(x)e^{-\Lambda n}$ and the orthonormality properties of the Legendre polynomials, giving the following identities:

$$\int_0^\pi d\xi \sin \xi P_\ell(\cos \xi) \frac{1}{\sqrt{\cosh \Lambda - \cos \xi}} = \frac{\sqrt{2}}{\lambda_\ell} e^{-\lambda_\ell \Lambda},$$

$$\int_0^\pi d\xi \sin \xi P_\ell(\cos \xi) \frac{1}{(\cosh \Lambda - \cos \xi)^{3/2}} = \frac{2\sqrt{2}}{\sinh \Lambda} e^{-\lambda_\ell \Lambda}.$$

After performing these integrations Eq. (C1) reduces to

$$E_{\text{eq-p}}^{s,s} = 2\pi \varepsilon_o a V_s^2 \sum_{\ell=0}^{\infty} e^{-2\lambda_\ell \Lambda} (\coth \lambda_\ell \Lambda + 1)$$

$$= 2\pi \varepsilon_o a V_s^2 \sum_{\ell=0}^{\infty} \frac{e^{-\lambda_\ell \Lambda}}{\sinh \lambda_\ell \Lambda}. \quad (\text{C2})$$

Note that the previous equation can be written as

$$E_{\text{eq-p}}^{s,s} = 2\pi \varepsilon_o a V_s^2 \sum_{\ell=1}^{\infty} \left[\frac{e^{-\ell \frac{\Lambda}{2}}}{\sinh \ell \frac{\Lambda}{2}} - \frac{e^{-\ell \Lambda}}{\sinh \ell \Lambda} \right], \quad (\text{C3})$$

which after some rearrangement reduces to the well-known form for the energy for the prescribed case of equipotentials [24]:

$$E_{\text{eq-p}}^{s,s} = 2\pi \varepsilon_o V_s^2 a \sum_{n=1}^{\infty} \frac{1}{\sinh \Lambda n}. \quad (\text{C4})$$

With the same identities one can derive the other terms contributing to the electrostatic energy. The cross terms are

given by

$$E_{\text{eq-p}}^{s,p} = E_{\text{eq-p}}^{p,s} = -2\pi \varepsilon_o a V_s V_p \sum_{\ell=0}^{\infty} \frac{e^{-\lambda_\ell \Lambda}}{\sinh \lambda_\ell \Lambda}, \quad (\text{C5})$$

and the component depending on the square of the plane's potential can be written as

$$E_{\text{eq-p}}^{p,p} = 2\pi \varepsilon_o a V_p^2 \sum_{\ell=0}^{\infty} \coth \lambda_\ell \Lambda. \quad (\text{C6})$$

The contribution to the electrostatic energy from the preceding equation contains a divergence which results from the infinite self-energy of the plane. Note from Eq. (A11) and using Eq. (C2) that for the case of an equipotential on the plane the plane self-energy reduces to $E_{\text{eq-p,self-energy}}^{p,p} = 2\pi \varepsilon_o a V_p^2 \sum_{\ell=0}^{\infty} 1$. By subtracting this divergence the plane-plane contribution to the electrostatic energy becomes

$$E_{\text{eq-p}}^{p,p} - E_{\text{eq-p,self-energy}}^{p,p} = 2\pi \varepsilon_o a V_p^2 \sum_{\ell=0}^{\infty} \frac{2}{e^{2\lambda_\ell \Lambda} - 1}$$

$$= 2\pi \varepsilon_o a V_p^2 \sum_{\ell=0}^{\infty} \frac{e^{-\lambda_\ell \Lambda}}{\sinh \lambda_\ell \Lambda}. \quad (\text{C7})$$

By combining all of the terms which contribute to the energy after all divergences have been removed we find the final form for the equipotential energy:

$$E_{\text{eq-p}} = 2\pi \varepsilon_o (V_s - V_p)^2 a \sum_{n=1}^{\infty} \frac{1}{\sinh \Lambda n}. \quad (\text{C8})$$

For completeness we should point out that the energy above still contains the finite and distance independent self-energy of the sphere. The expression for the force in the equipotential case can be derived by taking a derivative with respect to sphere-plane separation, giving

$$F_{\text{eq-p}} = -2\pi \varepsilon_o (V_s - V_p)^2 \sum_{n=1}^{\infty} \frac{\coth \Lambda - n \coth \Lambda n}{\sinh \Lambda n}, \quad (\text{C9})$$

which, as expected, agrees with the known results [24].

-
- [1] R. Smoluchowski, *Phys. Rev.* **60**, 661 (1941).
 [2] N. Gaillard *et al.*, *Appl. Phys. Lett.* **89**, 154101 (2006).
 [3] T. W. Darling, Ph.D. thesis, University of Melbourne, Australia, 1989.
 [4] J. B. Camp, T. W. Darling, and R. E. Brown, *J. Appl. Phys.* **69**, 7126 (1991).
 [5] F. Rossi and G. I. Opat, *J. Phys. D: Appl. Phys.* **25**, 1349 (1992).
 [6] T. W. Darling, F. Rossi, G. I. Opat, and G. F. Moorhead, *Rev. Mod. Phys.* **64**, 237 (1992).
 [7] T. C. Leung, C. L. Kao, W. S. Su, Y. J. Feng, and C. T. Chan, *Phys. Rev. B* **68**, 195408 (2003).
 [8] Y. Pu, D. D. Neufeld, and F. B. Dunning, *Phys. Rev. A* **81**, 042904 (2010).
 [9] F. C. Witteborn and W. M. Fairbank, *Phys. Rev. Lett.* **19**, 1049 (1967).
 [10] N. A. Robertson *et al.*, *Classical Quantum Gravity* **23**, 2665 (2006).
 [11] S. E. Pollack, S. Schlamminger, and J. H. Gundlach, *Phys. Rev. Lett.* **101**, 071101 (2008).
 [12] C. W. F. Everitt *et al.*, *Phys. Rev. Lett.* **106**, 221101 (2011).
 [13] R. D. Reasenberg *et al.*, *Classical Quantum Gravity* **28**, 094014 (2011).
 [14] L. Deslauriers, S. Olmschenk, D. Stick, W. K. Hensinger, J. Sterk, and C. Monroe, *Phys. Rev. Lett.* **97**, 103007 (2006).
 [15] R. J. Epstein *et al.*, *Phys. Rev. A* **76**, 033411 (2007).
 [16] A. Safavi-Naini, P. Rabl, P. F. Weck, and H. R. Sadeghpour, *Phys. Rev. A* **84**, 023412 (2011).
 [17] J. D. Carter and J. D. D. Martin, *Phys. Rev. A* **83**, 032902 (2011).
 [18] C. C. Speake and C. Trenkel, *Phys. Rev. Lett.* **90**, 160403 (2003).
 [19] W. J. Kim, A. O. Sushkov, D. A. R. Dalvit, and S. K. Lamoreaux, *Phys. Rev. A* **81**, 022505 (2010).
 [20] W. J. Kim and U. Schwarz, *J. Vac. Sci. Technol. B* **28**, 3 (2010).

- [21] S. K. Lamoreaux, in *Casimir Physics*, edited by D. A. R. Dalvit, P. W. Milonni, D. C. Roberts, and F. S. S. Rosa, Lecture Notes in Physics Vol. 834 (Springer-Verlag, Heidelberg, 2011), Chap. 7.
- [22] S. K. Lamoreaux and A. O. Sushkov, [arXiv:1106.3549](https://arxiv.org/abs/1106.3549).
- [23] R. O. Behunin, F. Intravaia, D. A. R. Dalvit, P. A. Neto, and S. Reynaud, *Phys. Rev. A* **85**, 012504 (2012).
- [24] W. R. Smythe, *Static and Dynamic Electricity* (McGraw-Hill, New York, 1950).
- [25] W. J. Kim, A. O. Sushkov, D. A. R. Dalvit, and S. K. Lamoreaux, *Phys. Rev. Lett.* **103**, 060401 (2009).
- [26] A. O. Sushkov, W. J. Kim, D. A. R. Dalvit, and S. K. Lamoreaux, *Nat. Phys.* **7**, 230 (2011).
- [27] P. M. Morse and H. Feschbach, *Methods of Theoretical Physics, Part II* (Feschbach, Minneapolis, 1981).
- [28] I. S. Gradshteyn and I. M. Ryzhik, *Table of Integrals, Series, and Products* (Academic Press, London, 1994).
- [29] To understand this point consider a single patch on the plane with constant potential. Let us assume that its central point is described by $x\hat{x}$. In bispherical coordinates this point is equivalent to $\frac{a \sin \xi \cos \phi}{1 - \cos \xi} \hat{x}$. In polar coordinates the central position of this patch is independent of the sphere-plane distance. Alternatively, the patch's position described by bispherical coordinates changes as we alter the sphere-plane separation (note the dependence of a on D). Therefore, if one were to compute the force by taking the derivative of Eq. (11) derivatives of the potentials on each object would appear in the final expression.
- [30] N. E. Singh-Miller and N. Marzari, *Phys. Rev. B* **80**, 235407 (2009).